Atomic-Scale Structure of Nanocrystals by High-Energy X-ray Diffraction and Atomic Pair Distribution Function Analysis: Study of Fe_xPd_{100-x} ($x = 0, 26, 28, 48$) Nanoparticles

V. Petkov,*,† T. Ohta,‡ Y. Hou,§ and Y. Ren||

Department of Physics, Central Michigan University, Mt. Pleasant, Michigan 48859, Department of Chemistry, School of Science, The University of Tokyo, Tokyo 113-0033, Japan, Department of Chemistry, Brown University, Providence, Rhode Island 02912, and X-ray Science Division, Advanced Photon Source, Argonne National Laboratory, Argonne, Illinois 60439

Received: September 20, 2006; In Final Form: October 24, 2006

Knowledge of the atomic-scale structure is an important prerequisite to understanding and predicting properties of materials. With bulk crystals it is routinely obtained by X-ray diffraction. With nanocrystals, however, traditional X-ray crystallography fails because of their substantially limited length of structural coherence. Here we illustrate, step by step, how a nontraditional approach involving high-energy X-ray diffraction and atomic pair distribution function analysis is applied to determine the atomic-scale structure of a typical nanocrystalline material—Fe_xPd_{100-x} ($x = 0, 26, 28, 48$) nanoparticles exhibiting useful magnetic properties.

I. Introduction

X-ray diffraction has long been used to determine the atomic-scale structure of materials. The technique is based on the fact that the wavelength of X-rays is comparable in size to the distances between atoms in condensed matter. Thus, when a bulk material that exhibits a long-range, periodic atomic order, such as a crystal, is irradiated with X-rays, it acts as an extended, almost perfect grating and produces a diffraction pattern showing numerous sharp spots, called Bragg diffraction peaks. By measuring and analyzing the positions and intensities of Bragg peaks, it is possible to determine the spatial characteristics of the grating, i.e. to determine the three-dimensional (3D) atomic arrangement in bulk crystals. This is the essence of the so-called "crystal structure" determination by X-ray diffraction (XRD).[1] X-ray diffraction has been successfully applied to study the atomic arrangement in bulk materials exhibiting a very short range (usually less than a nanometer), nonperiodic atomic ordering (e.g., glasses, liquids) as well. Atoms in such materials act as an extended but very imperfect grating when irradiated with X-rays and produce XRD patterns that are very diffuse in nature. A specialized approach, known as the atomic pair distribution function (PDF) technique, has been developed to analyze diffuse (i.e., non-Bragg type) XRD patterns and obtain important structural information for bulk noncrystalline materials such as near atomic neighbor separations and coordination numbers.[2] Thus X-ray diffraction has proven to be a valuable research tool in science and technology of both bulk crystals and noncrystals. Recent rapid development of nanoscience and nanotechnology, however, has posed new challenges to the atomic-scale structure determination by X-ray diffraction. As their name implies, nanocrystals are of sizes ranging from 1 nm to several nanometers. Furthermore, inside a nanocrystal atoms may be ordered over distances that are even shorter than its size. As a result, nanocrystals act as a limited and, very often, a not quite perfect grating and, hence, produce XRD patterns showing both Bragg-like peaks and a diffuse component (see Figure 1a). The Bragg-like peaks are, however, not as sharp and not as many as those observed in the XRD pattern of bulk crystals. Also, the diffuse component is very strong, similar to what is observed with bulk noncrystals, and may not be neglected. This renders the traditional (Bragg) X-ray crystallography very difficult to apply. Here we show how a combination of high-energy XRD and PDF data analysis can be used to determine the atomic-scale structure of nanocrystals in detail. As an example, we study a typical nanocrystalline material being developed for practical applications—Fe_xPd_{100-x} ($x = 0, 26, 28, 48$) nanoparticles. Due to their high magnetocrystalline anisotropy and chemical stability, bulk crystalline FePd alloys have generated much interest for high-density data storage applications.[3] Recently the attention has shifted to FePd nanoparticles because they offer a significant improvement in hard disk drive data storage capacity. The aim is to obtain FePd nanoparticles with a desired size, composition, and atomic-scale structure that is known to promote their useful magnetic properties. The success of this effort depends critically on the accessibility of 3D atomic arrangement.

II. Experimental Section

II.1. Sample Preparation and Characterization. Fe_xPd_{100-x} nanoparticles were prepared via a wet chemical route based on the reduction of Pd(acetylacetonate)$_2$ with hexadecanediol and thermal decomposition of $Fe(CO)_5$. The size and composition of the nanoparticles were controlled by using appropriate stabilizers and adjusting the reaction conditions. For example, with 4:1 molar ratio of $Fe(CO)_5$ to Pd(acetylacetonate)$_2$, $Fe_{28}Pd_{72}$ nanoparticles were produced using oleic acid−tributylphosphone as a stabilizer, while $Fe_{48}Pd_{52}$ nanoparticles were produced using adamantanelcarboxylic acid−tributylphosphone as a stabilizer. The chemical composition of each sample was checked by energy dispersive X-ray analysis. More details of the preparation route can be found in ref 4. Tranmission electron microscopic (TEM) experiments[4] showed that Fe_xPd_{100-x} nanoparticles were nearly spherical in shape, were almost monodis-

* Corresponding author. E-mail: petkov@phy.cmich.edu.
† Central Michigan University.
‡ The University of Tokyo.
§ Brown University.
|| Argonne National Laboratory.

10.1021/jp066166p CCC: $37.00
Published on Web 12/07/2006

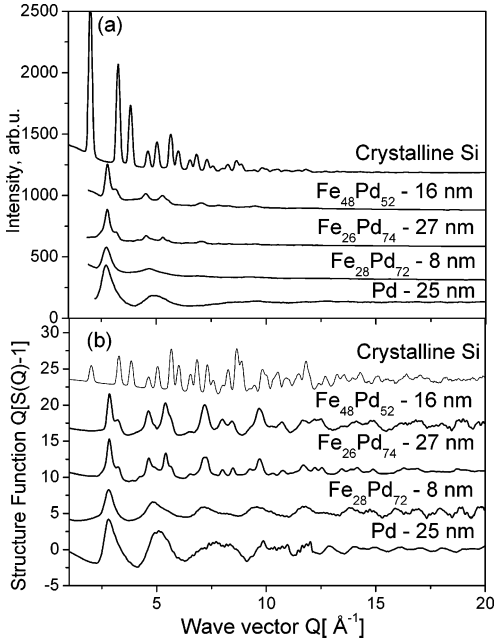

Figure 1. Background (hexane, air, and sample holder) corrected, high-energy XRD patterns (a) and corresponding structure functions (b) for Fe_xPd_{100-x} nanoparticles and bulk crystalline Si.

perse, and had an average size of approximately 5, 27, 8, and 16 nm for $x = 0$, 26, 28 and 48, respectively. Like many others, we too found TEM indispensable in determining the nanoparticle size and shape. TEM images are, however, a projection down an axis and, therefore, are not quite sensitive to the 3D atomic arrangement inside materials. High-energy X-rays, due to their high penetration depth, nondestructively probe the interior of materials and are much more informative in this respect.

II.2. High-Energy XRD Measurements. High-energy XRD experiments were carried out at the 11-ID-C beamline (Advanced Photon Source, Argonne National Laboratory) using synchrotron radiation of energy 114.496 keV ($\lambda = 0.1083$ Å) at room temperature. Since nanoparticles have been found to change structure in response to changes in environment,[5] the XRD measurements were carried out on Fe_xPd_{100-x} nanoparticles as obtained and stored in hexane. Pure hexane and bulk crystalline Si were also measured and used to estimate the "nanoparticle background" scattering and evaluate the optical alignment of the experimental setup, respectively. All samples were sealed in glass capillaries. The scattered radiation was collected with an imaging plate (IP) detector (mar345). Up to 10 images were taken for each of the samples. Thanks to the high flux of the synchrotron source and the large area detector employed, the exposure time was reduced to 10 s per image.[6] The as-collected (two-dimensional, 2D) images were combined, subjected to geometric corrections, integrated, and reduced to one-dimensional XRD patterns, shown in Figure 1a, with the help of the computer program FIT2D.[7] As can be seen, the XRD pattern for crystalline Si shows numerous sharp Bragg peaks to wave vectors as high as 10 $Å^{-1}$, as might be expected for a material exhibiting a long-range, periodic atomic order. Such a diffraction pattern lends itself to atomic-scale structure determination by the traditional crystallographic approach.[1,8] The XRD patterns of nanoparticles, however, show only a few broad Bragg-like peaks that merge into a slow-oscillating diffuse component already at Q-values as low as 5−7 $Å^{-1}$ and may not be straightforwardly analyzed in the traditional way. Besides, the setting of magnetically most useful face centered cubic/face centered tetragonal (fcc/fct) phases in FePd crystals is signaled by the appearance of extra, so-called superlattice peaks in the XRD patterns, reflecting the setting of chemical ordering.[9] Competing but less magnetically useful phases are chemically disordered and do not show such peaks. The rather diffuse nature of the XRD patterns of Fe_xPd_{100-x} nanoparticles makes it impossible to detect neither "superlattice" peaks" nor local tetragonal distortions, i.e., to detect any signatures of chemical ordering. As we illustrate here, the problem can be solved by going beyond the traditional crystallography and using the atomic PDF data analysis approach.

II.3. PDF Analysis: Basics. Although atomic PDF analysis has been around for a while, it has not been as widely recognized and used in structure studies of nanocrystals as it could be. That is why its essentials are described here in brief.

The frequently used reduced atomic PDF, $G(r)$, gives the number of atoms in a spherical shell of unit thickness at a distance r from a reference atom as follows:

$$G(r) = 4\pi r[\rho(r) - \rho_o] \tag{1}$$

where $\rho(r)$ and ρ_o are the local and average atomic number densities, respectively, and r is the radial distance. As defined, the PDF $G(r)$ is a one-dimensional function that oscillates around zero and shows positive peaks at distances separating pairs of atoms, i.e., where the local atomic density exceeds the average one. The negative valleys in the PDF correspond to real-space vectors not having atoms at either of their ends. In this respect the PDF resembles the so-called Patterson function that is widely applied in traditional X-ray crystallography.[1] However, while the Patterson function is discrete and peaks at interatomic distances within the unit cell of a crystal, the atomic PDF is a continuous function peaking at all interatomc distances occurring in materials. This is an important advantage when the physical dimensions of and/or the degree of atomic ordering and periodicity in materials are substantially limited as in nanocrystals. The PDF $G(r)$ is the Fourier transform of the experimentally observable total structure function, $S(Q)$, i.e.

$$G(r) = (2/\pi) \int_{Q=0}^{Q_{max}} Q[S(Q) - 1] \sin(Qr)\, dQ \tag{2}$$

where Q is the magnitude of the wave vector ($Q = 4\pi \sin\theta/\lambda$), 2θ is the angle between the incoming and outgoing X-rays, and λ is the wavelength of the X-rays used.[2] X-ray diffraction usually employs the so-called Faber−Ziman type structure function, $S(Q)$, related to the coherent part of the diffraction pattern, $I^{coh}(Q)$, as follows:

$$S(Q) = 1 + [I^{coh}(Q) - \sum c_i |f_i(Q)|^2]/|\sum c_i f_i(Q)|^2 \tag{3}$$

where c_i and $f_i(Q)$ are the atomic concentration and X-ray scattering factor, respectively, for the atomic species of type i.[2,10] It should be noted that for a material comprising n atomic species a single diffraction experiment yields a total atomic distribution function, $G(r)$, which is a weighted sum of $n(n + 1)/2$ partial PDFs, $G(r_{ij})$, i.e.

$$G(r) = \sum_{i,j} w_{ij} G_{ij}(r) \tag{4}$$

Here w_{ij}'s are weighting factors depending on the concentration and scattering power of the atomic species as follows:

$$w_{ij} = c_i c_j f_i(Q)\, f_j(Q)/\sum [c_i f_i(Q)]^2 \tag{5}$$

For practical purposes w_{ij}'s are often evaluated for $Q = 0$.[2,10] As can be seen from eqs 1−5, $G(r)$ is simply another representation of the experimental XRD data. However, exploring the XRD data in real space is advantageous, especially in the case of materials exhibiting a substantially limited length of structural coherence, such as nanocrystals. First, as eq 3 implies, the *total* scattering, including Bragg-like peaks as well as diffuse (non-Bragg-like) scattering, contributes to the PDF. In this way both the yet measurable atomic order, manifested in the Bragg-like peaks, and all structural "imperfections" that are responsible for its limited extent, manifested in the intense diffuse component of the diffraction pattern, are reflected in the experimental PDF. Second, by accessing high values of Q, experimental $G(r)$ values of improved real-space resolution[11] can be obtained and, hence, quite fine details in the atomic-scale structure revealed. In fact, data at high Q values ($Q > 10$ Å^{-1}) are critical to the success of PDF analysis. Diffraction data at high wave vectors are easily obtained using X-rays of a shorter wavelength, i.e., of higher energy (see the definition of the wave vector Q). In laboratory conditions such X-rays are produced by standard X-ray tubes with a Mo or Ag anode.[2] Modern sources of high-energy X-rays such as synchrotrons may also be employed. Third, $G(r)$ is barely influenced by diffraction optics and experimental factors since these are accounted for in the step of extracting the coherent intensities from the raw XRD data (see eq 3). This makes the PDF an experimental quantity that gives directly relative positions of atoms enabling a convenient determination of important structural parameters (e.g., coordination numbers and distances) as well as testing and refinement of 3D structural models.

The experimental XRD patterns of Fe_xPd_{100-x} nanoparticles were subject to due corrections, normalized into absolute units (i.e., converted to $I^{coh}(Q)$), reduced to structure functions $S(Q)$ (see eq 3), and then Fourier transformed to atomic PDFs (see eq 2) with the help of the program RAD.[12]

Thus obtained reduced structure functions $Q[S(Q) - 1]$ are shown in Figure 1b, and the corresponding atomic PDFs are shown in Figure 2. As can be seen in Figure 1b, all structure functions exhibit physical (i.e., not noise-based) oscillations to the maximum value of 20 Å^{-1} reached with the present experiments. The higher frequency oscillations (coming from the Bragg-like peaks in the XRD data) reflect the longer range atomic order. The low-frequency ones (coming from the diffuse-like component in the XRD data) reflect the structural imperfections that limit this order. Note that many physical oscillations in the XRD patterns remain "hidden" when the data are analyzed in the traditional way (Figure 1a) but are clearly revealed in the corresponding reduced structure functions (see Figure 1b). This is one of the major differences between the traditional X-ray crystallography and the high-energy XRD coupled to a PDF-based data analysis approach. While the former relies mostly on sharp and intense Bragg peaks appearing at low-Q values and, hence, is mostly sensitive to the long-range, periodic atomic order, the latter uses all physical oscillations (information) stored in the diffraction data and, hence, is sensitive to the atomic ordering of any extent and periodicity.[1,2,10,11] This is well demonstrated by the experimental atomic PDFs. As can be seen in Figure 2, the experimental PDF for crystalline Si shows a series of well-defined peaks to quite long real-space distances, as it should be with a material exhibiting a long-range, periodic atomic order (i.e., a long length of structural coherence). The PDFs for Fe_xPd_{100-x} nanoparticles also exhibit noticeable peaks, but those vanish already at approximately 1.0, 2.5, 1.2, and 3 nm for the samples with $x = 0$, 26, 28, and 48,

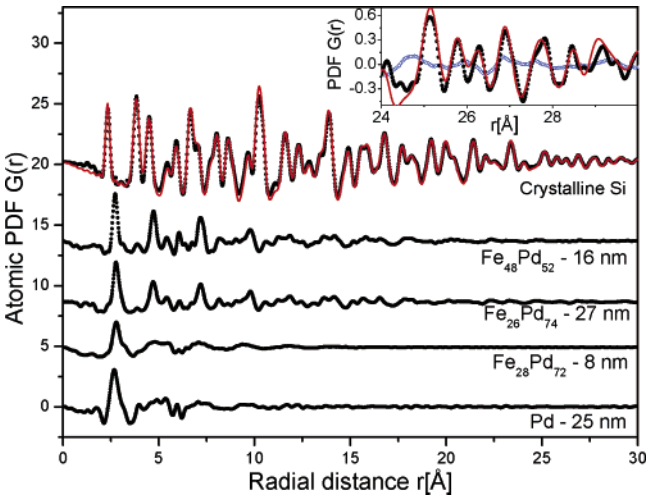

Figure 2. Atomic PDFs (solid circles) for Fe_xPd_{100-x} nanoparticles and crystalline Si extracted from the XRD data of Figure 1. The experimental PDF for crystalline Si is compared with a model one (solid line in red) computed on the basis of literature data for the structure of the bulk solid. The inset shows the higher-r region of the experimental and model data for Si on an enlarged scale. Note that the oscillations in the experimental data at high values of r are well reproduced by those in the model PDF, proving that these oscillations are a structurally relevant feature and not an experimental artifact. The experimental PDF for 27 nm $Fe_{26}Pd_{74}$ particles (symbols in blue) is also shown in the inset for comparison. It does not show physical oscillations for real-space distances longer than 2.5 nm, while the PDF for a material with a long-range atomic-scale structure, such as bulk crystalline Si, does.

respectively. Obviously, the nanoparticles exhibit an atomic ordering that is well-defined at distances from 1 nm up to a few nanometers but lack the extended order (structural coherence) of usual crystals. Here it should be noted that the atomic PDFs for the nanoparticles decay to almost zero at interatomic distances that are much shorter than the average nanoparticle size determined by TEM. The difference is due to the fact that TEM yields the nanoparticle size while high-energy XRD and PDF yield the nanoparticle average length of structural coherence. When atoms in nanoparticles constitute a single, coherently scattering X-ray domain, the nanoparticle size and length of structural coherence may coincide; otherwise they may not. Our studies show that Fe_xPd_{100-x} nanoparticles, obtained and stored in hexane, are very likely to possess a multidomain structure. It is well-known that the presence of distinct structural domains influences some structure-dependent properties of materials, especially the magnetic ones. The ability to reveal the presence of domains in nanocrystals, and yield an estimate for their size, is another important advantage of the high-energy XRD and PDF analysis approach.

II.4. PDF Analysis: Application. As can be seen in Figure 2, the peaks in the different experimental PDFs, with different amplitudes and/or positions, show that the 3D atomic arrangement in each of the materials studied is different. The first peak in the experimental PDF for Si is positioned at 2.35 Å, which is exactly the first atomic neighbor distance in crystalline Si. The average first coordination number, estimated from the area of the first PDF peak, is four. This is the first coordination number in bulk crystalline Si known to have a relatively open, diamond-type structure. A model PDF based on this structure type (space group $Fd\bar{3}m$, lattice parameter $a = 5.431$ Å)[13] is also shown in Figure 2. It was computed on the basis of literature data (unit cell constants and atomic positions) for the structure of crystalline Si, including data for the root-mean-square (rms) atomic vibrations at room temperature. The calculations were done with the help of the program PDFFIT.[14] The effect of the

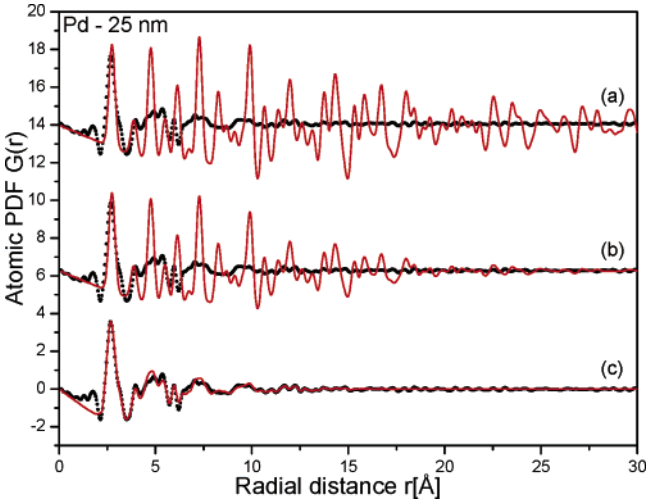

Figure 3. Experimental (symbols) atomic PDF for 25 nm Pd particles and model PDFs (solid lines in red) for a long-range and periodic, fcc-type structure occurring with crystalline Pd (a), hypothetical Pd nanoparticles with only a size-limited fcc-type structure (b), and heavily disordered (noncrystalline/nonperiodic) Pd nanoparticles (c). Examples of the corresponding model atomic configurations are shown in Figure 4.

instrument/detector resolution on the PDF data was taken into account as described in refs 3 and 10. As can be seen, the experimental and model PDFs for bulk crystalline Si agree very well up to high interatomic distances (see the inset in Figure 2). The agreement well documents the fact that atomic PDFs accurately reflect the 3D atomic arrangement in materials and thus may serve as a reliable basis for its determination. Indeed, the approach of using a structure-sensitive, one-dimensional experimental quantity (e.g., the profile of Bragg peaks) to construct and test 3D atomic models is widely applied in traditional crystal structure determination from powder XRD data.[1,8] Here the quantity is the atomic PDF and the 3D atomic-scale structure of nanocrystals is being sought.

The first peaks in the experimental PDFs for Fe_xPd_{100-x} nanoparticles are positioned at 2.67, 2.78, and 2.72 Å for $x =$ 0, 26/28, and 48 (see Figure 2). Those are the typical first neighbor atomic distances in the corresponding bulk crystalline alloys. The positions of the subsequent atomic coordination spheres in the nanoparticles, estimated from the positions of the subsequent peaks in the experimental PDFs, also resemble those observed in Fe_xPd_{100-x} bulk crystals.[9,15−17] These observations suggest that the atomic arrangements in Fe_xPd_{100-x} nanoparticles and bulk crystals are likely to share similar characteristics. Therefore, atomic arrangements already found in Fe_xPd_{100-x} crystals may be a good starting point for the search for structure models of the corresponding nanoparticles. Finding a reasonable initial model for the nanoparticle's atomic-scale structure may not have been so straightforward if the almost featureless XRD patterns and not the corresponding atomic PDFs were considered. With the results of the preliminary analysis of the experimental PDFs at hand, we approached pure Pd nanoparticles ($x = 0$) with a model based on the fcc-type atomic structure found in bulk crystalline Pd.[16] A comparison between the experimental PDF for 25 nm Pd particles and a model one for a material exhibiting the long-range, fcc-type structure of crystalline Pd is shown in Figure 3a. A fragment of the structure is shown in Figure 4a. The calculations were again done with the help of the program PDFFIT using literature data for crystalline Pd. As can be seen in Figure 3a, the first peaks in the model and experimental PDF data agree well in both position and intensity, indicating that both Pd nanoparticles and bulk crystals have almost the same immediate atomic ordering (first atomic coordination sphere). As can be expected, however, the model and experimental data disagree at higher-r distances, clearly showing that Pd nanoparticles do not exhibit the long-range, periodic atomic order of bulk Pd crystals. Another model PDF was also computed, this time for hypothetical Pd nanoparticles differing from bulk Pd in size but not in atomic-scale struture. The size-limited length of structural coherence in such Pd nanoparticles was modeled by multiplying the model PDF data for bulk Pd with a decaying exponent as suggested in ref 18 and implemented in ref 5. The effect of the correction is to depress the PDF uniformly without changing its shape. As can be seen in Figure 3b, the real Pd nanoparticles we studied do not seem to exhibit only a size-limited atomic order of a fcc-type, either. Instead, as can be seen in Figure 3c, the very rapid decay of the physical oscillations in the experimental PDF, i.e., the very limited length of structural coherence in 27 nm Pd particles, is well reproduced by a model representing a heavily disordered, almost random packing of atoms (see Figure 4c). The model was generated via a reverse Monte Carlo type procedure involving placing Pd atoms in a simulation box and moving them around so that the difference between the model and experimental PDF data becomes as small as possible. The calculations were done with the help of the program DISCUS.[19]

The experimental PDF for 8 nm $Fe_{28}Pd_{72}$ particles is also very well reproduced by a model showing a very high degree of structural disorder (see Figure 5b). This model was generated via a reverse Monte Carlo type procedure involving placing an appropriate amount of Pd and Fe atoms in a simulation box and moving them around so that the difference between the model and the corresponding experimental PDF data becomes as small as possible. To check for possible chemical order/disorder effects, Fe and Pd atoms were also allowed to swap their positions in the simulation box at the final stages of the modeling. The calculations were done with the help of the program DISCUS.[19] As the simulations show, a heavily disordered atomic arrangement where pairs of like atoms (e.g., Fe−Fe and Pd−Pd pairs) occur more often than usual does a better job in reproducing some fine details in the experimental PDF data than a similar atomic arrangement where Fe and Pd species are distributed at random (see the inset in Figure 5b). The generated models for structurally heavily disordered $Fe_{28}Pd_{72}$ nanoparticles with and without a preferential arrangement of Fe and Pd species about each other, i.e., with or without chemical ordering, are shown in part d and c, respectively, of Figure 6. As the data in Figure 5a show, 27 nm $Fe_{26}Pd_{74}$ particles exhibit a range of structural coherence (~2.5 nm) that is almost twice that of 8 nm $Fe_{28}Pd_{72}$ particles (~1.2 nm). Also, the atomic arrangement in 27 nm $Fe_{26}Pd_{74}$ particles appears very similar to that found in bulk crystalline $FePd_3$,as calculations carried out with PDFFIT show. Here again a periodic model exhibiting chemical ordering (space group $Pm\bar{3}m$, lattice parameter $a =$ 3.84(1) Å; see Figure 6b) does a better job in reproducing the fine details in the experimental data than a chemically disordered one (space group $Fm\bar{3}m$, lattice parameter $a = 2.72(1)$ Å; see Figure 6a). It should be clarified that the observed differences between the chemically ordered and disordered models, manifested by the differences in the corresponding model PDFs, are relatively small with $Fe_{28}Pd_{72}$ and $Fe_{26}Pd_{74}$ nanoparticles because the atomic correlations involving Fe atoms have a relatively small contribution ($w_{Fe-Fe} = 2.5\%$, $w_{Fe-Pd} \sim 8\%$) to the experimental PDF data. When necessary, the sensitivity of atomic PDFs to a particular type of atomic species may be

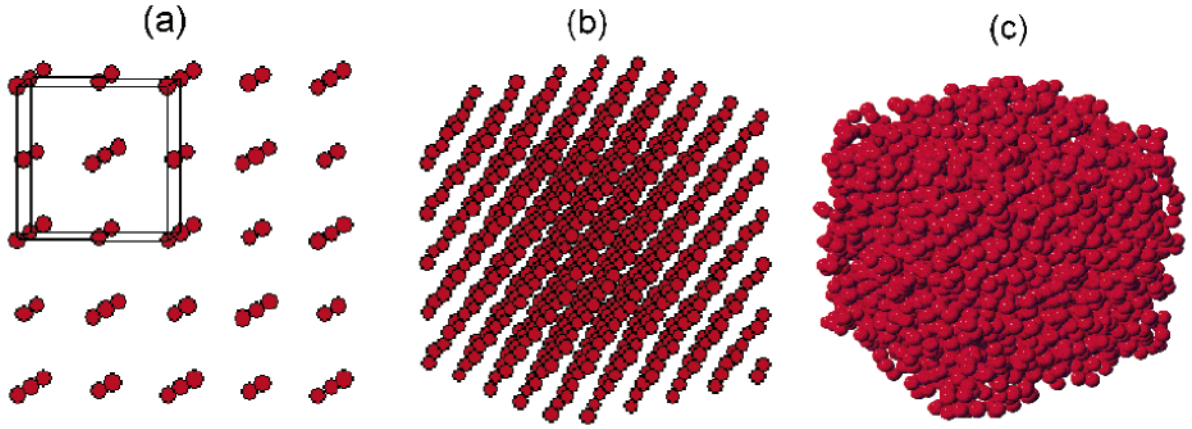

Figure 4. Fragment of the "infinite" (periodic) fcc-type structure occurring with crystalline Pd (a). The corresponding unit cell is outlined with solid lines. Pd nanoparticle with only size-limited fcc-type structural features (b). A heavily disordered (i.e., noncrystalline) Pd nanoparticle (c). Pd atoms are presented as circles (in red).

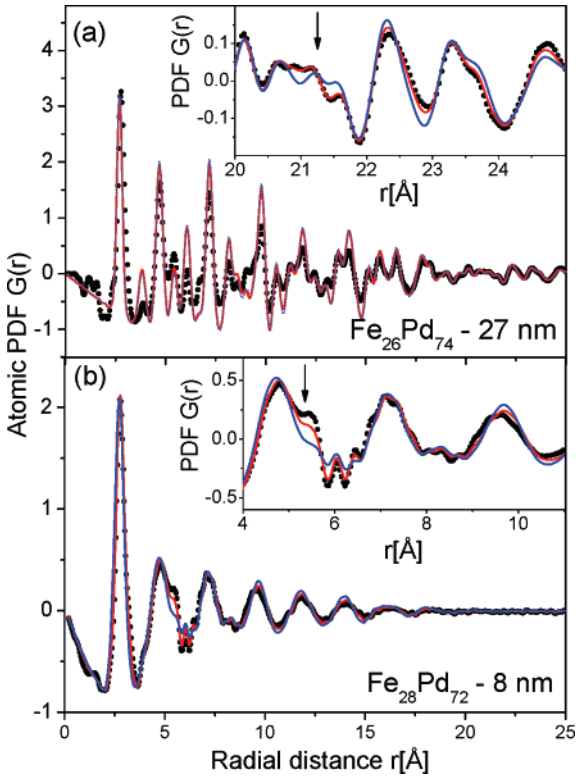

Figure 5. Experimental (symbols) atomic PDFs for 27 nm $Fe_{26}Pd_{74}$ (a) and 8 nm $Fe_{28}Pd_{72}$ (b) particles. In (a) the experimental data are compared with model ones for chemically disordered (line in blue) and chemically ordered (line in red) nanoparticles exhibiting a periodic atomic ordering of the type found in chemically disordered and ordered $FePd_3$ crystals, respectively. In (b) a comparison is made with model PDFs for chemically disordered (line in blue) and chemically ordered (line in red) nanoparticles exhibiting a heavily disordered (i.e., a noncrystalline/nonperiodic) atomic-scale structure. The respective model atomic configurations are shown in Figure 6. The insets show the higher-r portion of the data on an enlarged scale. Arrows mark experimental PDF features that are reproduced better by the chemically ordered structure models.

increased substantially by tuning the energy of X-rays used close to an absorption edge of that species, i.e., by employing resonant X-ray diffraction.[20] With $Fe_{48}Pd_{52}$ nanoparticles the contribution of Fe involving atomic pairs to the experimental PDF data is larger ($w_{Fe-Fe} = 13\%$ and $w_{Fe-Pd} = 23\%$), making it easier to check for the presence of chemical ordering. As can be seen in Figure 7, the atomic ordering in 16 nm $Fe_{48}Pd_{52}$ particles appears very close to that found in bulk crystalline FePd. Here, a

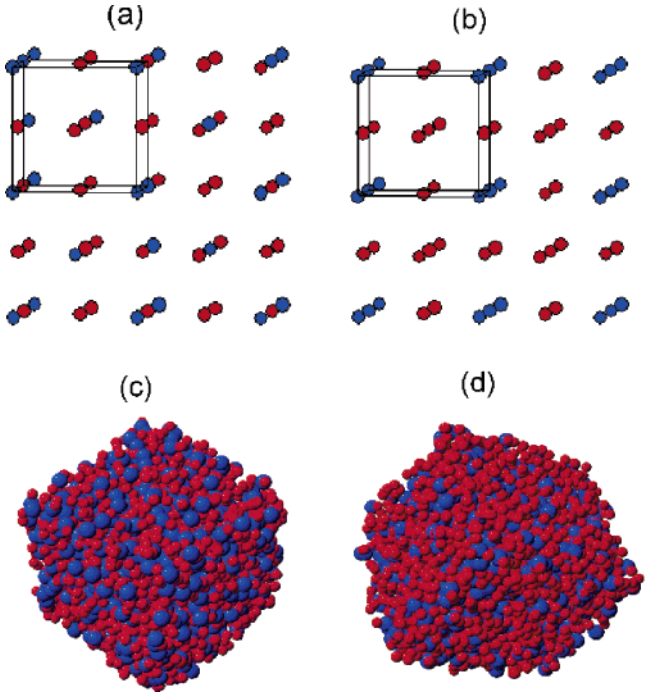

Figure 6. Fragments of the "infinite" (periodic) fcc-type structures occurring with chemically disordered (a) and ordered (b) bulk $FePd_3$ crystals. The corresponding unit cells are outlined with solid lines. Models for chemically disordered (c) and chemically ordered (d) $Fe_{28}Pd_{72}$ nanoparticles exhibiting a very high degree of structural disorder. Pd and Fe atoms are presented as red and blue circles, respectively.

chemically ordered and periodic atomic arrangement of a tetragonal type (space group $P4/mmm$, lattice parameters $a = 2.72(1)$ Å and $c = 3.72(1)$ Å; see Figure 8b) reproduces well all important details in the experimental PDF, especially at longer real-space distances (see the inset in Figure 7). A chemically disordered one of a cubic, fcc type (space group $Fm\bar{3}m$, lattice parameter $a = 3.80(1)$ Å; see Figure 8a) clearly does not reproduce the experimental data so well.

III. Discussion

High-energy XRD and PDF studies reveal the following characteristic features of the atomic-scale structure of Fe_xPd_{100-x} nanoparticles ($x = 0$, 26, 28, 48): Atoms in 25 nm Pd particles ($x = 0$) are ordered over very short distances as usually found in noncrystals (e.g., metallic glasses). The same is true for 8 nm $Fe_{28}Pd_{72}$ particles. Increasing the nanoparticle's size (from

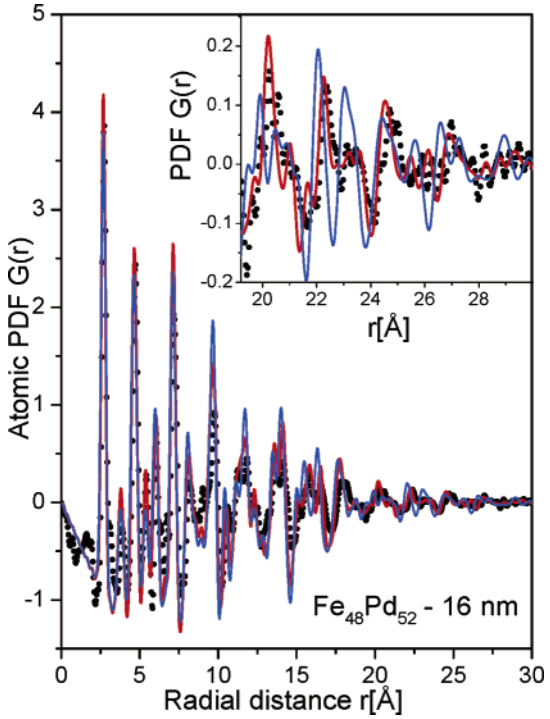

Figure 7. Experimental (symbols) atomic PDF for 16 nm $Fe_{48}Pd_{52}$ particles. The experimental data are compared with model ones for chemically disordered (solid line in blue) and chemically ordered (solid line in red) nanoparticles exhibiting a periodic atomic arrangement of the type found in chemically disordered and ordered bulk FePd crystals, respectively. Fragments of the 3D structure of chemically ordered (fct-type) and chemically disordered (fcc-type) bulk FePd crystals are shown in Figure 8. The inset shows the higher-*r* portion of the experimental and model data on an enlarged scale.

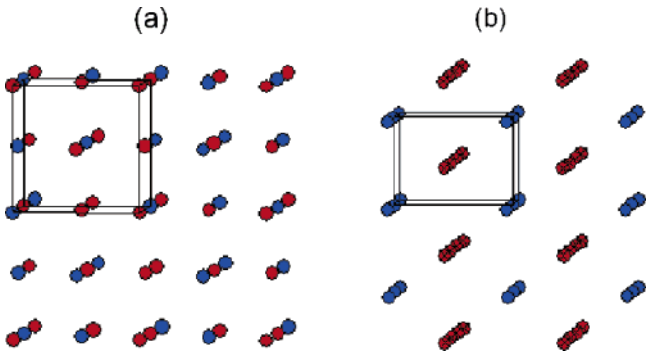

Figure 8. Fragments from the "infinite" (periodic) fcc-type (a) and fct-type (b) atomic arrangements occurring with chemically disordered (a) and chemically ordered (b) bulk FePd crystals. The corresponding unit cells are outlined with solid lines. Pd and Fe atoms are presented as red and blue circles, respectively.

8 nm with $Fe_{28}Pd_{72}$ particles to 27 nm with $Fe_{26}Pd_{74}$ particles) while keeping the chemical composition almost the same results in a considerable increase in the length of structural coherence. Alloying Pd with more Fe ($Fe_{48}Pd_{52}$ versus $Fe_{28}Pd_{72}$ particles) also results in a measurable increase in the length of structural coherence. In all cases, however, the length of structural coherence is much shorter than the average nanoparticle size. Furthermore, Fe and Pd atomic species in Fe_xPd_{100-x} nanoparticles ($x = 26, 28, 48$) obviously do not mix at random but prefer to arrange in a particular pattern with respect to each other. How the exact degree of chemical ordering is, when necessary, evaluated is shown in our recent high-energy XRD and PDF studies on Cu_3Au.[21] When nanoparticles/nanocrystals exhibit a very short (~1 nm or so) length of structural coherence, as is the case with 25 nm Pd and 8 nm $Fe_{28}Pd_{72}$ particles, heavily disordered, nonperiodic atomic configurations may provide a good description of the atomic-scale structure. Such models are usually employed to describe the structure of "noncrystals" and possess a great number of parameters including the coordinates and chemical type of all atoms in the atomic configuration. On the other hand, when nanoparticles/nanocrystals exhibit a length of structural coherence of at least a few nanometers, as is the case with 27 nm $Fe_{26}Pd_{74}$ and 16 nm $Fe_{48}Pd_{52}$ particles, models that are periodic atomic arrangements of the type usually employed to describe the atomic-scale structure of "crystals" may do a good job. The latter structure models possess a relatively small number of parameters (the unit cell of the periodic atomic arrangement with its symmetry and the positions and type of the atoms within it) and are thus more convenient in calculating and predicting the structure-dependent properties of nanocrystals.[22] However, calculations of structure-dependent properties may not always be necessary to be done in order to reveal structure−property relations in nanocrystals. Quite often, structure knowledge provided by high-energy XRD experiments and PDF analyses, as it is, may be used to assess properties of nanocrystals and/or streamline a nanotechnology process. For example, to obtain the magnetically most useful, chemically ordered phase, the as-synthesized Fe_xPd_{100-x} ($x = 48$) nanoparticles typically are annealed at elevated temperatures. At the annealing temperatures the surfactants used to stabilize the nanoparticles usually break down, exposing the nanoparticle's surface. This frequently results in a noticeable agglomeration of the nanoparticles and a drastic increase in their size distribution, spoiling the data storage capacity. However, as the results of our PDF study show, the present nanotechnological route yields $Fe_{48}Pd_{52}$ particles that exhibit a tetragonal-type structure involving a significant chemical ordering as obtained, and, therefore, may not require a prolonged postannealing at elevated temperatures. It may be noted that signatures of chemical ordering may also be detected and/or some understanding about the immediate atomic ordering in nanocrystals obtained by analyzing first atomic neighbor coordination numbers and distances yielded by X-ray absorption spectroscopy experiments.[23] However, only the high-energy XRD and PDF approach can reveal both the chemical and spatial ordering of atoms in nanocrystals over the entire length of structural coherence they show. Nanoparticles, inorganic and metallic, have also shown improved catalytic[24] and optical processes,[25] and are often a product of geochemical[26] or environmental remediation processes.[27] Structural information of the type obtained here may be indispensable in all these fields of nanoparticle research and technology.

IV. Conclusion

Fe_xPd_{100-x} nanoparticles of different sizes, degrees of structural coherence, and prominent chemical ordering may be obtained by the wet nanotechnological route described in this work. Detailed information about the 3D atomic arrangement inside the nanoparticles may be obtained by employing a nontraditional experimental approach—high-energy XRD and atomic PDF analysis. This information provides an atomic-scale view of the product of the route, helping to steer it better toward obtaining a nanomaterial with a desired functionality.

From a somewhat more general point of view, the present study is a convincing demonstration of the ability of high-energy XRD and PDF analysis to yield detailed knowledge of the 3D atomic arrangement in nanocrystalline materials exhibiting any range of structural coherence and periodicity. Using a combina-

tion of high-energy XRD and PDF analysis, we have very recently determined the atomic-scale structure of nanotubes,[28] nanoceramics,[29] inorganic/organic nanocomposites,[30] and nanosize organic molecules used for drug delivery.[31] The demonstrated success and marked flexibility with respect to the sample's state, morphology, amount, and environment, the ability to do time-depended studies, and the ability to employ either laboratory equipment or state-of-the-art synchrotrons are all very appealing evidence for the great capabilities of this nontraditional experimental approach. We believe that it has the potential to become the "standard tool" for atomic-scale structure determination that is highly needed in the rapidly developing field of nanoscience and technology.[32]

Acknowledgment. Thanks are due to M. Beno from APS, Argonne National Laboratory, for the help with the synchrotron experiments. The work was supported by NSF through Grant DMR 0304391(NIRT) and CMU through Grant REF C602281. The Advanced Photon Source is supported by DOE under Contract No. DE-AC02-06CH11357.

References and Notes

(1) Giacovazzo, C.; et al. In *Fundamentals of x-ray crystallography*; Oxford University Press: New York, 1998.

(2) Klug, H. P.; Alexander, L. E. In *X-ray diffraction procedures for polycrystalline and amorphous materials*; John Wiley & Sons: New York, 1974.

(3) Ristou, R. A.; et al. *J. Appl. Phys.* **1999**, *86*, 4527−4533.

(4) Hou, Y.; et al. *Chem. Mater.* **2004**, *16*, 5149−5152.

(5) Zhang, H.; et al. *Nature* **2003**, *424*, 1025−1029.

(6) For comparison, experimental data of similar quality would have taken a few days to be obtained with an in-house source of X-rays. It is obviously advantageous, but not absolutely necessary, to use synchrotron sources of high-energy X-rays in PDF studies of nanocrystals.

(7) Hammersley, A. P. Report ESRFF97HA02T; Grenoble, France, 1997.

(8) Pecharsky, V. K.; Zavalij, P. Y. In *Fundamentals of powder diffraction and structural characterization of materials*; Kluwer Academic Publishers: Norwell, MA, 2003.

(9) Longhorn, G. *Phys. Rev.* **1969**, *172*, 572−576. Wang, L.; Fan, Z.; Roy, A. C.; Laughlin, D. E. *J. Appl. Phys.* **2005**, *95*, 7483−7485.

(10) Egami, T.; Billinge, S. J. L. In *Underneath the Bragg Peaks*; Pergamon Press: Elmsford, NY, 2003.

(11) Petkov, V.; et al. *Phys. Rev. Lett.* **1999**, *83*, 4089−4092.

(12) Petkov, V. *J. Appl. Crystallogr.* **1989**, *22*, 387−389.

(13) Hubbard, C. R.; Swanson, H. E.; Mauer, F. A. *J. Appl. Crystallogr.* **1975**, *8*, 45−48.

(14) Proffen, Th.; Billinge, S. J. L. *J. Appl. Crystallogr.* **1999**, *32*, 572−575.

(15) Swanson, H. E.; Tatge, E. *Natl. Bur. Stand. Circ. (U.S.)* **1953**, *359*, 11−195.

(16) Jaeaeskelaeinen, J.; Suoninen, E. *Phys. Status Solidi* **1981**, *63*, 241−245.

(17) Hultgren, R.; Zappfe, C. A. *Fiz. Met. Metalloved.* **1976**, *99*, 57−62.

(18) Ergun, S.; Schehl, S. R. *Carbon* **1973**, *11*, 127−138.

(19) Proffen, Th.; Neder, R. B. *J. Appl. Crystallogr.* **1997**, *30*, 171−175.

(20) Fuoss, P. H.; Eisenberger, P.; Warburton, W. K.; Bienenstock, A. *Phys. Rev. Lett.* **1981**, *46*, 1537−1540.

(21) Proffen, Th.; Petkov, V.; Billinge, S. J. L.; Vogt, T. *Z. Kristallogr.* **2002**, *217*, 47−50.

(22) Petkov, V.; Billinge, S. J. L.; Larson, P.; Mahanti, S. D.; Vogt, T.; Rangan, K. K.; Kanatzidis, M. *Phys. Rev. B* **2002**, *65*, 092105(1-4.)

(23) Hwang, B.-J.; et al. *J. Am. Chem. Soc.* **2005**, *127*, 11140−11145.

(24) Chackroune, N.; et al. *Langmuir* **2005**, *21*, 6788−6796.

(25) Chuang, C. M.; et al. *J. Appl. Phys.* **2005**, *97*, 096104-7.

(26) Waychunas, G. A.; Kim, Ch. S.; Banfield, J. F. *J. Nanopart. Res.* **2005**, *7*, 409−433.

(27) Billinge, S. J. L.; McKimmy, E. J.; Ahatnawi, M.; Kim, H.-J.; Petkov, V.; Wermeille, D.; Pinnavaia, T. J. *J. Am. Chem. Soc.* **2005**, *127*, 8492−8498.

(28) Petkov, V.; Zavalij, P. Y.; Lutta, S.; Whittingham, M. S.; Parvanov, V.; Shastri, S. *Phys. Rev. B* **2004**, *69*, 085410(1-6).

(29) Petkov, V.; Gateshki, M.; Niederberger, M.; Ren, Y. *Chem. Mater.* **2006**, *18*, 814−821.

(30) Petkov, V.; Parvanov, V.; Trikalitis, P.; Malliakas, Ch.; Vogt, T.; Kanatzidis, M. *J. Am. Chem. Soc.* **2005**, *127*, 8805−8812.

(31) Petkov, V.; Parvanov, V.; Tomalia, D.; Swanson, D.; Bergstrom, D.; Vogt, T. *Solid State Commun.* **2005**, *134*, 671−675.

(32) Worked-out examples of high-energy XRD and PDF studies on nanocrystals, relevant software and literature can be found at http://phy.cmich.edu/people/petkov/x-ray/nanocrystals/.